An algorithm for subtraction of doublet emission lines in angle-resolved photoemission spectroscopy

Yaoju Tarn [a], Mekhola Sinha [b], Christopher Pasco [b], Darrell G. Schlom [c,d], Tyrel M. McQueen [b,d], Kyle M. Shen [a], Brendan D. Faeth [a,d,*]

[a] Department of Physics, Laboratory of Atomic and Solid State Physics, Cornell University, Ithaca, NY, 14853, USA
[b] Department of Chemistry, Johns Hopkins University, Baltimore, MD, 21218, USA
[c] Department of Materials Science and Engineering, Cornell University, Ithaca, NY, 14853, USA
[d] Platform for the Accelerated Realization, Analysis, and Discovery of Interface Materials (PARADIM), Cornell University, Ithaca, NY, 14853, USA

ARTICLE INFO

ABSTRACT

Plasma discharge lamps are widely utilized in the practice of angle-resolved photoemission spectroscopy (ARPES) experiments as narrow-linewidth ultraviolet photon sources. However, many emission lines such as Ar-I, Ne-I, and Ne-II have closely spaced doublet emission lines, which result in superimposed replica on the measured ARPES spectra. Here, we present a simple method for subtracting the contribution of these doublet emission lines from photoemission spectra. Benchmarking against ARPES spectra of well-characterized 2D materials, we demonstrate that this algorithm manages to subtract the doublet signal and reproduce the key features of the monochromated He-Iα spectra in a physically sound manner that reliably reproduces quantifiable dispersion relations and quasiparticle lifetimes.

1. Introduction

Angle-resolved photoemission spectroscopy (ARPES) is a powerful tool in modern experimental condensed matter physics for characterizing the electronic structure of quantum materials [1–3]. A key component of any ARPES system is the light source, the characteristics of which determine much of the system's experimental capabilities. The beam profile, photon polarization, and incident flux of the photon source determines the effective spatial resolution, orbital sensitivity, and photoemission signal intensity, respectively. Meanwhile, the photon energy $h\nu$ serves as a critical parameter in determining the probed out-of-plane momentum $k_\perp$. It is for this reason that high-intensity, continuously tunable synchrotron radiation sources are strongly preferred for band mapping of 3D materials. In contrast, lab-based ARPES systems frequently rely on noble gas discharge lamps which produce a series of intense narrow emission lines at discrete photon energies depending on the gas plasma used. The most common emission lines are He-Iα at 21.2 eV and He-IIα at 40.8 eV.

Other gases can also be used to generate useful discharge lines at 8.4 eV (Xe I) [4,5], 10 eV (Kr-I) [6], 11.8 eV (Ar-I) [7], 16.8 eV (Ne-I), and 26.9 eV (Ne-II). Unfortunately, many of these discharge spectra include secondary "doublet" lines of comparable intensity and with narrow energy spacings [8] less than the 1.5 eV that a typical lab-based vacuum ultraviolet (VUV) monochromator is able to effectively filter,

resulting in a shifted, overlapping signal in the measured photoemission spectra.

The challenge of using such doublet emission lines for ARPES experiments is illustrated in Fig. 1. Our experimental system consists of a high resolution hemispherical electron analyzer (Scienta Omicron DA30-L), a toroidal monochromator (Scienta Omicron VUV 5040), and a multi-gas RF discharge lamp (Fermion Instruments BL1200s). In Fig. 1(a), we show VUV discharge spectra measured with this system from a polycrystalline gold reference sample using Kr, Ar, He, and Ne plasma. The peak intensity profiles shown are generated by taking the derivative of an angle-integrated Fermi edge collected at 6 K. Even with the monochromator, substantial secondary lines at lower $h\nu$ remain for Ar-I [Fig. 1(b)], Ne-I [Fig. 1(c)], and Ne-II [Fig. 1(d)]. The effect of these secondary lines on measured ARPES spectra is clearly demonstrated in Fig. 1(e) and (f), which show unprocessed ARPES spectra of a cleaved Bi$_2$Se$_3$ single crystal at Γ [9] using both monochromated Kr-Iα 10eV photons [Fig. 1(e)] and Ne-I doublet emission [Fig. 1(f)]. In the latter case, the measured spectra exhibits a pair of overlapping, duplicate copies, with the weaker Ne-Iβ signal appearing at lower kinetic energy. The presence of this overlapping doublet signal is highly problematic, particularly when attempting to extract quantitative parameters such as dispersion relations and quasiparticle lifetimes from ARPES spectra.

---

* Corresponding author at: Department of Physics, Laboratory of Atomic and Solid State Physics, Cornell University, Ithaca, NY, 14853, USA.
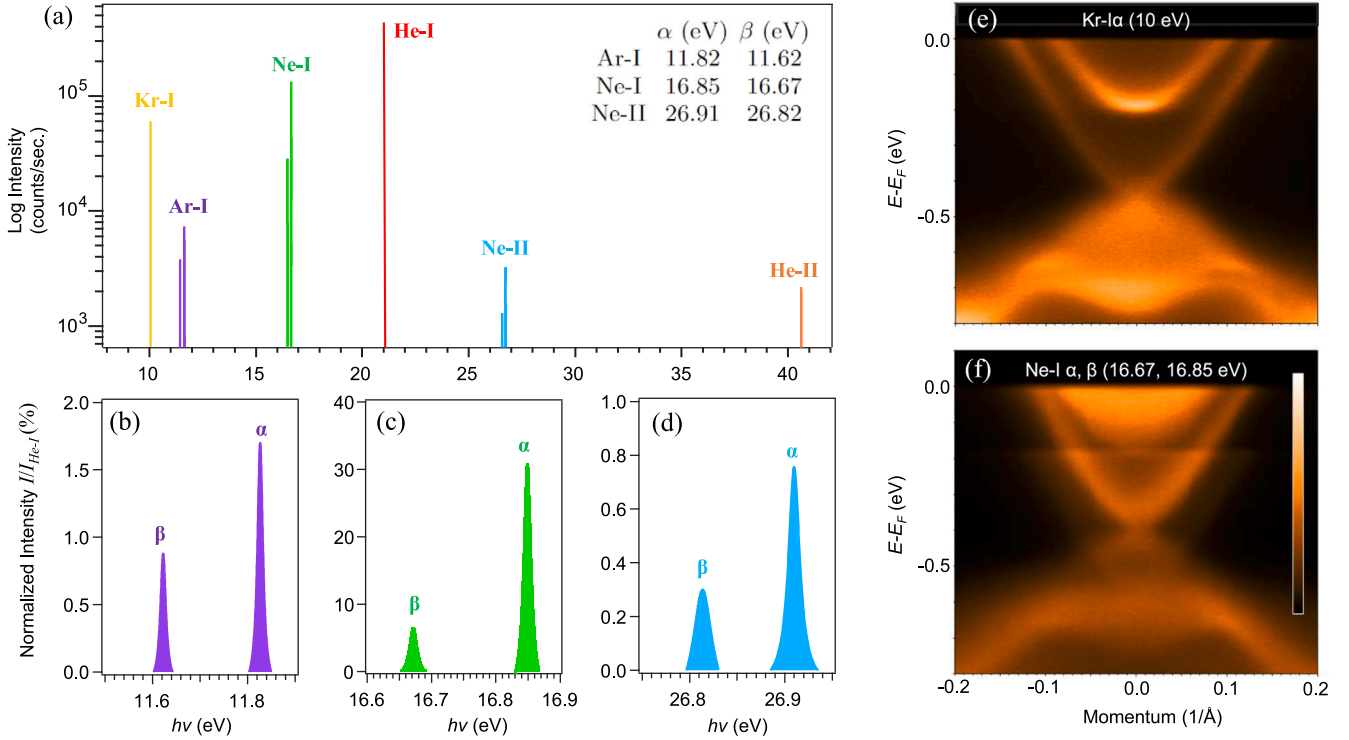*E-mail addresses:* yt493@cornell.edu (Y. Tarn), bdf53@cornell.edu (B.D. Faeth).

Fig. 1. (a) Discharge spectra of Kr, He, Ne, and Ar gases after filtering through a Scienta Omicron VUV 5040 toroidal monochromator. Spectra are generated by taking the derivative of the angle-integrated Fermi Edge of a poly-crystalline Au sample. See Appendix A for additional details. (b)–(d) Magnified view of the Ar-I, Ne-I, and Ne-II emission lines, normalized to the intensity of He-I. (e)–(f) ARPES spectra of Bi_2Se_3 obtained using Kr and Ne-I gases, respectively. The Kr discharge is passed through a CaF filter to produce a discrete 10 eV source, whereas the Ne-I light is imperfectly selected with the monochromator and retains signal from both Ne-Iα and Ne-Iβ.

Consequently, there is a need for a method to eliminate the β line contribution from ARPES spectra collected using doublet emission sources. In this work, we present a simple method for performing such a subtraction based on a piece-wise reconstruction algorithm.

2. Subtracting the doublet photoemission signal

In a conventional photoemission experiment using a monochromatic photon source with energy $h\nu$, the relationship between the measured kinetic energy ω of the outgoing electrons and the original binding energy E_B is

$$\omega = h\nu - \phi_A - E_B, \qquad (1)$$

where ϕ_A is the known work function of the electron analyzer. When a doublet photon source is used, the measured photoemission signal I_{tot} becomes a superposition of the emission from both lines, such that

$$I_{tot}(\mathbf{k}, \omega) = \alpha(\mathbf{k}, \omega) + \beta(\mathbf{k}, \omega), \qquad (2)$$

where $\alpha(\mathbf{k}, \omega)$ and $\beta(\mathbf{k}, \omega)$ are the α and β signal's contribution to the total intensity at the measured kinetic energy ω and momentum $\mathbf{k}$.

We now consider a simplified scenario, in which the measured spectral intensity scales directly with the photon flux for a given discharge line, but that the binding-energy dependent lineshapes are identical. In this situation, the overall signal $I_{tot}(\omega)$ at a fixed $\mathbf{k}$ can be written as

$$I_{tot}(\omega) = \alpha(\omega) + \beta(\omega) = \alpha(\omega) + R\alpha(\omega + \Delta E), \qquad (3)$$

where R is simply the fractional intensity ratio of the β photon flux to that of the more intense α line, and $\Delta E = h\nu_\alpha - h\nu_\beta$ is the doublet energy separation.

A solution for the isolated $\alpha(\omega)$ signal can be determined algorithmically from raw ARPES spectra using the form of Eq. (3) so long as ΔE and R are known accurately. We show this process diagrammatically in Fig. 2. We start by accounting for background above the Fermi level

as well as detector non-linearity [10] in the ARPES spectra and extract their energy distribution curves (EDCs). ΔE is determined using a Fermi edge fit [Fig. 2(a)]. ΔE is a property of the chosen noble gas discharge line and does not change between experiments. In the case of Fig. 2, Ne-I has a ΔE of 176 meV.

Next, we define a sub-range of the original EDC in a small window $[E_F - \frac{\Delta E}{2}, E_F + \frac{\Delta E}{2}]$ straddling the Fermi level of the α signal [Fig. 2(b)]. Within this energy range the contribution of the β signal is negligible. This EDC segment, denoted as $\alpha_0(\omega)$, is then translated by the energy separation ΔE and scaled by the intensity ratio R to produce $\beta_0(\omega) = R\alpha_0(\omega + \Delta E)$, representing the binding energy equivalent segment of the doublet β signal. The contribution of this doublet that extends into the domain of $\alpha_0(\omega)$ is then subtracted [Fig. 2(c)], leaving $\alpha_1(\omega) = \alpha_0(\omega) - \beta_0(\omega)$ as a pure state of the α signal. This process of subtraction is subsequently repeated over the index n, stitching window-by-window to the domain, until it has run through the full EDC. Mathematically, the flow goes as such, with E_F set to 0 for simplicity:

$$\alpha_0(\omega) = I_{tot}(\omega), \ \omega \in [-\frac{\Delta E}{2}, \frac{\Delta E}{2}] \qquad (4)$$

$$\beta_n(\omega) = R\alpha_n(\omega + \Delta E), \ \omega \in [-(n + \frac{1}{2})\Delta E, \frac{\Delta E}{2}] \qquad (5)$$

$$\alpha_{n \geq 1}(\omega) = I_{tot}(\omega) - \beta_{n-1}(\omega), \ \omega \in [-(n + \frac{1}{2})\Delta E, \frac{\Delta E}{2}] \qquad (6)$$

It is important to note that R can vary between experiments and is affected by numerous settings such as the monochromator setting and lamp pressure. For example, with Ne-I, we find that this intensity ratio R can vary over a range of ± 0.04. To account for this, we have an iterative step that varies R [Fig. 2(d)] to minimize the discontinuity. If R is determined incorrectly, a discontinuity remains, as seen in the purple curve [Fig. 2(d)]. This discontinuity is eliminated in the green curve of Fig. 2(d), where the output EDCs are fully decoupled from the β signal at the optimal R determined by this minimization. The process of removing this discontinuity is discussed in detail in Appendix B.
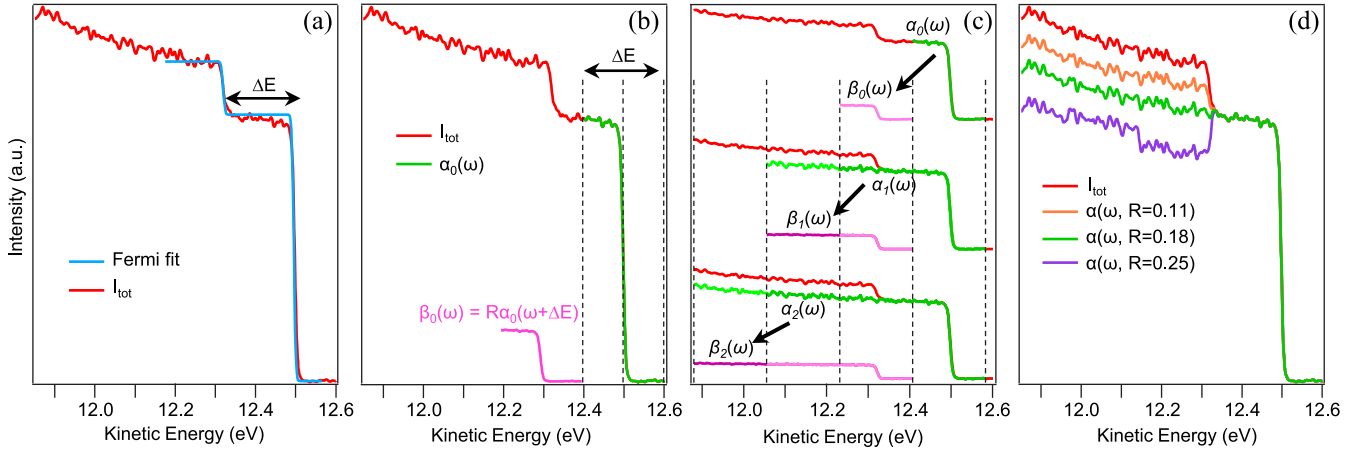
Fig. 2. Flowchart depicting how the full doublet subtraction method works, applied on an angle-integrated spectra from a polycrystalline copper sample measured with a Ne-I doublet as an example. (a) ΔE is extracted by a double Fermi edge fit on the integrated EDC. (b) $\alpha_0(\omega)$ (green curve) is initialized as the segment of the raw data (red curve) spanning a window of width ΔE, and $\beta_0(\omega)$ (pink curve) is initialized as a shifted and scaled copy of $\alpha_0(\omega)$. (c) $\beta_0(\omega)$ is subtracted from $\alpha_0(\omega)$ to generate $\alpha_1(\omega)$. The subtraction is repeated until it has covered the full range of the EDC. (d) The value of R is optimized by minimizing the discontinuity which appears at the boundary between the first and second segments, as detailed further in Appendix B. The optimal solution (green) has this discontinuity eliminated, while non-optimal solutions (purple and orange) continue to exhibit a discontinuity at ΔE below E_F.
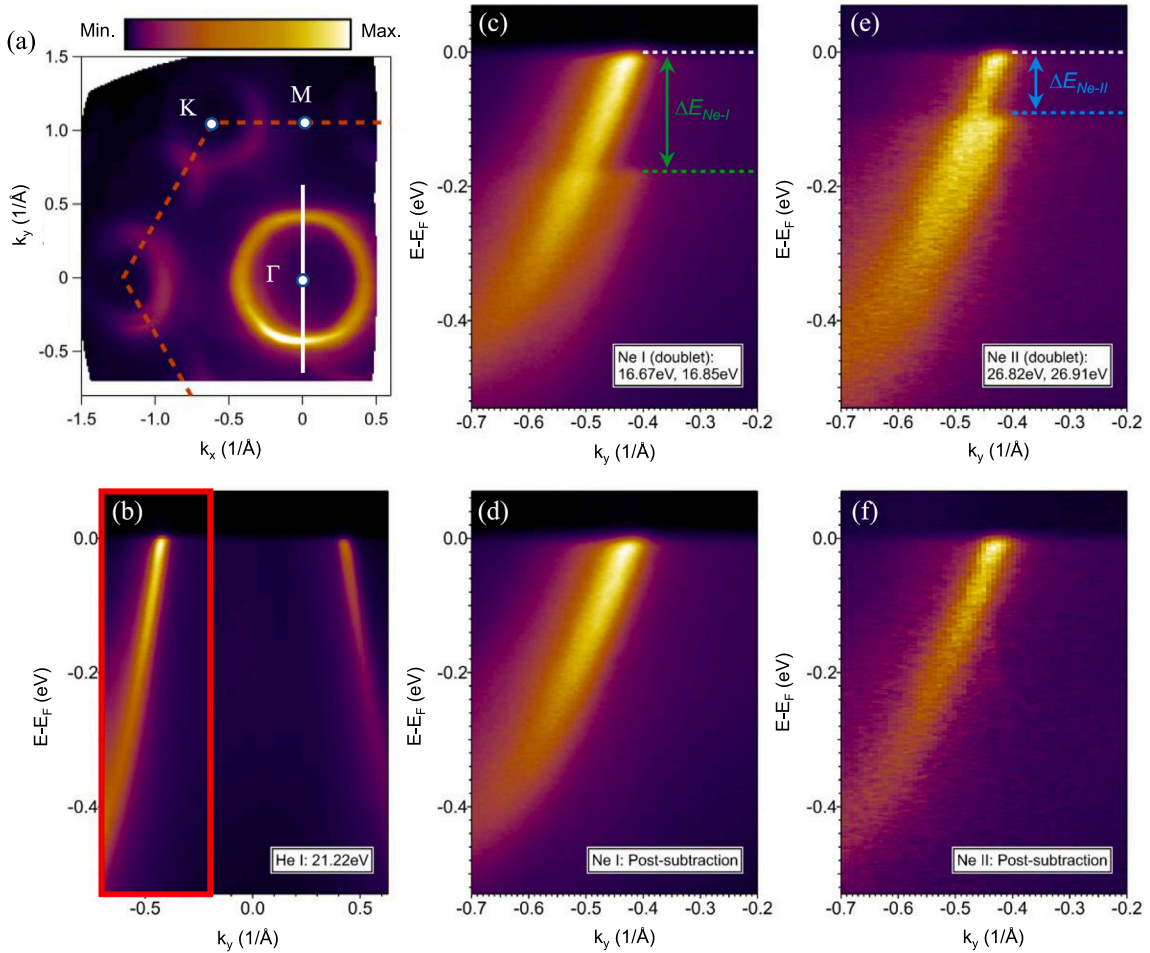

Fig. 3. (a) He-Iα Fermi surface intensity map of the cleaved surface of $(LaSe)_{1.14}(NbSe_2)_2$ single crystal, integrated over ± 5 meV of E_F. (b) Photoemission intensity at Γ point [white solid line in (a)] as measured with He-Iα radiation. Two branches of the hole pocket are visible, with the left band at negative k_y being more intense at this geometry. (c)–(d) Ne-I doublet spectra before and after subtraction, with green dotted line representing the second Fermi edge occurring at doublet separation energy of $\Delta E = 176$ meV (e)–(f) Ne-II doublet spectra before and after subtraction, with blue dotted line representing the second Fermi edge occurring at doublet separation energy of $\Delta E = 90$ meV.
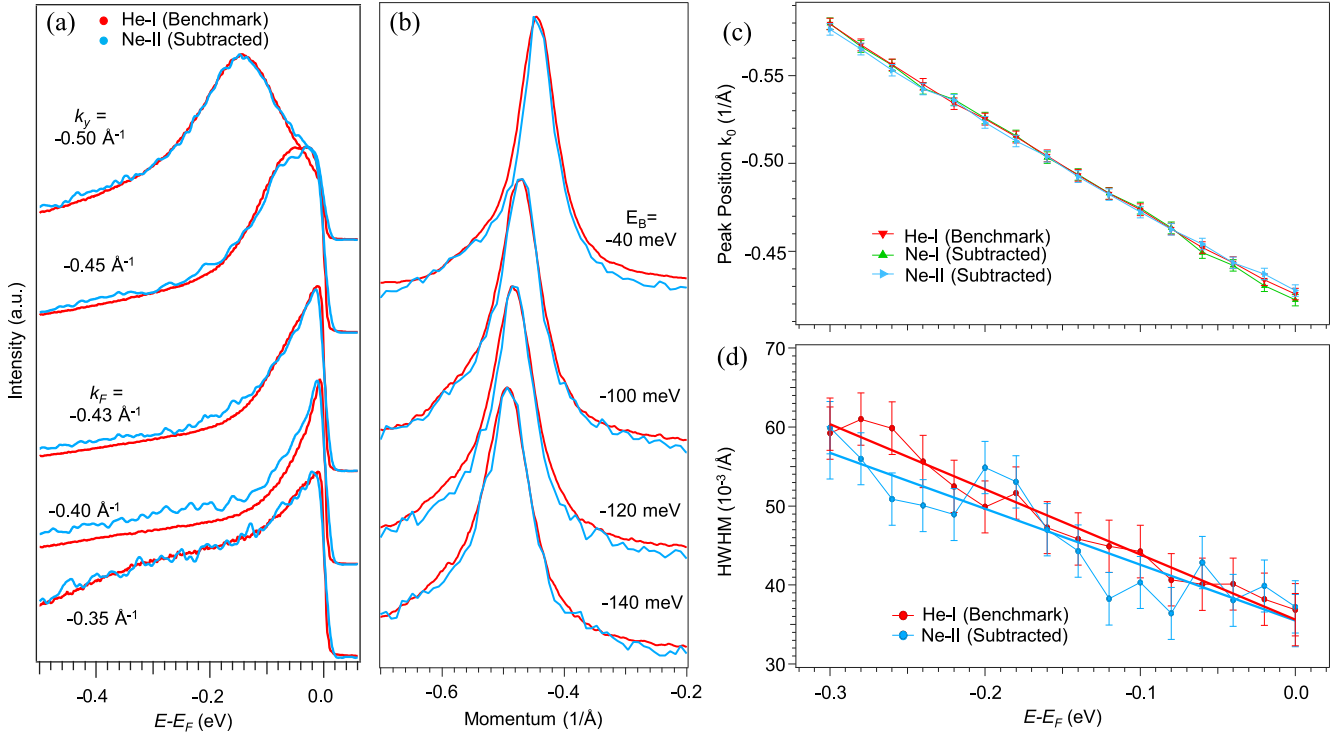
Fig. 4. (a) EDCs extracted from the He-I (red lines) and post-subtracted Ne-II (blue lines) spectra of Fig. 3(b and f) sampled at regular momenta from -0.5 to -0.35 Å^{-1}, as well as at the Fermi-crossing k_F at -0.43 Å^{-1}. Each EDC is averaged over a momentum range of 0.04 Å^{-1}. (b) MDCs extracted from He-I and post-subtracted Ne-II spectra at several representative binding energies. Each MDC is averaged over an energy range of 20 meV. (c) Dispersion relation (extracted from the data in Fig. 3(b,d,f)). (d) MDC width analysis on Fig. 3(b) and (f).

When working with a 2D spectra image as typically obtained by a standard hemispherical analyzer, it is necessary to first optimize R using either an integrated EDC from the bandmap itself or else using a reference spectra (typically a polycrystalline metallic Fermi edge) taken at the same instrumental conditions. Afterwards, that optimized R value is held constant as the subtraction algorithm is applied individually to each EDC in the original image, with the post-subtracted EDC's then re-constructed to obtain a final, post-subtracted 2D spectra.

3. Benchmarking performance

In order to characterize the performance of our algorithm, we performed ARPES measurements on the misfit layered compound $(LaSe)_{1.14}(NbSe_2)_2$, which has strong two-dimensional character and is therefore ideal for comparing measured spectra at different photon energies [11,12]. Single crystal samples were cleaved under good UHV conditions ($<6 \times 10^{-11}$ Torr) and measured at a temperature of 6 K with a nominal instrumental energy resolution of 6–10 meV for data taken with He-I and Ne-I, and 20 meV for data taken with Ne-II due to its reduced signal intensity.

In Fig. 3, we compare ARPES measurements of $(LaSe)_{1.14}(NbSe_2)_2$ using both monochromated and doublet emission sources to benchmark the efficacy of our subtraction algorithm. Fig. 3(a) shows the Fermi surface as measured with He-I, which consists of hole-like pockets at K and at Γ consistent with expectation for a heavily electron-doped $NbSe_2$ surface layer as observed in previous studies [12,13]. Fig. 3(b) shows a high-statistics energy–momentum image along the $\Gamma - M$ high symmetry direction of the $NbSe_2$ surface taken also with He-Iα radiation, showing a pair of well-isolated dispersive bands crossing the Fermi level, arising from Nb 4d states of the hole-like pocket centered on Γ.

The performance of our algorithm can be benchmarked directly by comparing processed ARPES images taken using doublet emission lines against this baseline monochromated He-I spectra. In Fig. 3(c,e) we show raw ARPES spectra along the same momentum cut and identical measurement geometry as the He-I spectra of Fig. 3(b), but taken with Ne-I and Ne-II emission, respectively. For clarity, we focus here on a single band crossing the Fermi level, as indicated by the narrower momentum window shown by the red box in Fig. 3(b). A second Fermi edge is visible for both raw spectra at an energy separation equal to ΔE, below which the duplicate superimposed features of the beta signal are clearly evident. In contrast, the algorithmically-subtracted doublet spectra shown in Fig. 3(d,f) show only a single sharp band without any obvious second Fermi edge or shadow band.

The lack of aberrations in the processed images is similarly clear when extracting quantitative features from the subtracted data. In Fig. 4, we present one-to-one comparisons of normalized EDCs [Fig. 4(a)] and MDCs [Fig. 4(b)] from the He-I (red lines) and post-subtracted Ne-II (blue lines) spectra of Fig. 3(b) and (f), taken at identical cuts in momenta and energy. We find that despite evidently greater measurement noise due to weaker signal intensity ($I_{Ne-II}/I_{He-I} < 1\%$), post-subtracted Ne-II EDCs and MDCs show nearly identical lineshapes to the He-I data, without any evident discontinuities or residual secondary peaks. This can also be seen in the measured dispersion relations and MDC linewidths presented in Fig. 4(c) and (d), respectively, which are extracted from Lorentzian fits to the He-I and post-subtracted Ne doublet data of Fig. 3. We note that the Ne-I data exhibited an additional unrelated shoulder in the MDC lineshape and was excluded from the comparison of Fig. 4(d) as a result. The fitted results for the subtracted data again exhibit near-perfect agreement with the He-I behavior within measurement uncertainty. Additionally, similar results were obtained when repeating the dispersion analysis on other cuts in momentum space, such as at the less intense band
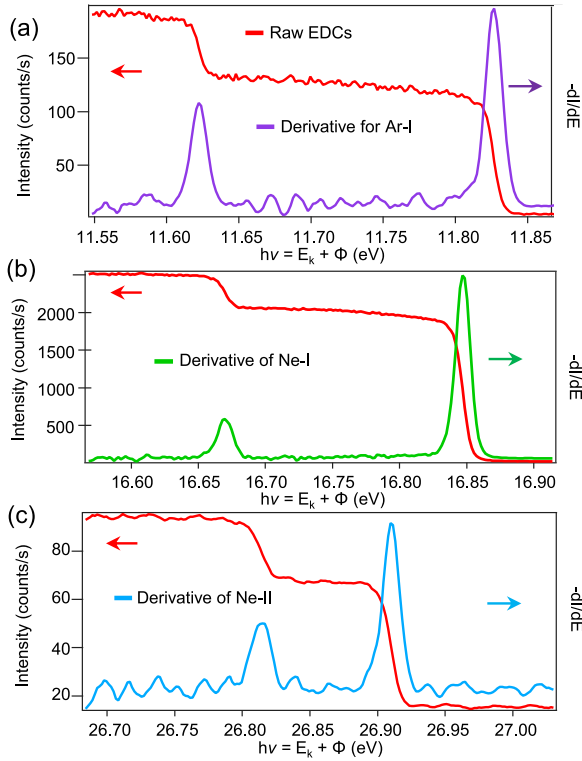
Fig. A.1. Emission spectra and the negative of their derivatives measured with monochromator set to (a) Ar-I, (b) Ne-I, (c) Ne-II. The raw integrated EDCs for each line are shown in red, and the negative derivatives are plotted against the right axes in purple, green, and blue for Ar-I, Ne-I, and Ne-II respectively. These peaks were fit with Lorentzians to obtain the strong emission lines shown in Fig. 1.
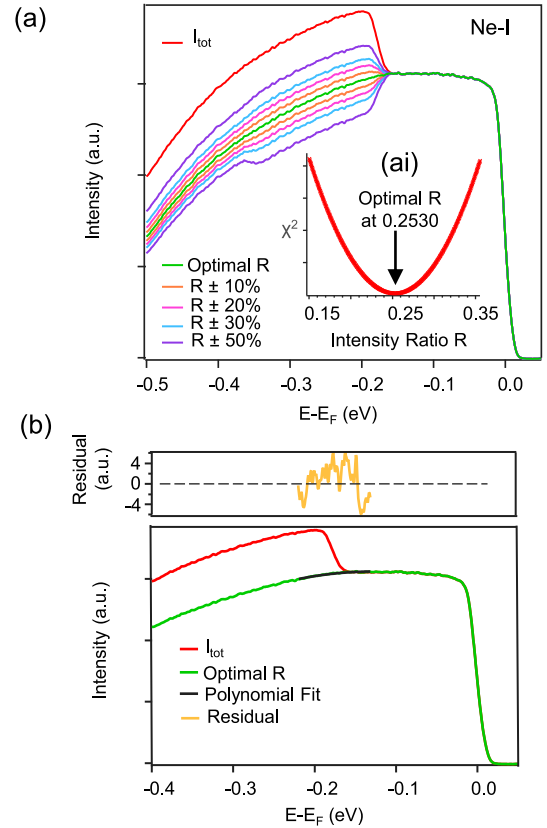

Fig. B.1. (a) Original and post-subtracted integrated EDCs extracted from the ARPES spectra of $(LaSe)_{1.14}(NbSe_2)_2$ misfit measured by Ne-I, which has a doublet separation of ΔE of 176 meV. Even slightly incorrect R of ± 10 percent creates discontinuities at around ΔE below E_F. (ai) Chi-squared values when varying over R to find the optimal solution for which the discontinuity is minimized. (b) A closer examination of the red and green curves in (a), along with the smooth curve against which the residual from iterating R is minimized. The yellow plot is the residual.

visible at positive k_y in Fig. 3(b). The excellent agreement across all measured and processed spectra demonstrates the practical efficacy of our algorithm at enabling quantitative analysis of ARPES spectra from doublet emission sources.

4. Discussion

It is worth noting that the simplified description of the doublet photoemission signal presented in Section 2 assumes that the binding-energy dependent EDC lineshapes of both the α and β signals are identical. In principle, however, the **k** position being sampled along an EDC on an ARPES image collected with a hemispherical analyzer varies with the kinetic energy in a fashion dependent on the exact measurement geometry [14,15]. A substantial variation in measured **k** between doublet line signals can in turn lead to differences in the intrinsic EDC lineshapes for the α and β signals in the case of highly dispersive band features. To evaluate the importance of this effect, we consider first the measured out-of-plane photoelectron momentum, given by

$$k_\perp = \sqrt{2m_e/\hbar^2}(V_0 + E_k \cos^2(\theta))^{1/2}, \tag{7}$$

where θ is the emission angle relative to normal and V_0 is the inner potential (typically ~10 eV). If we consider doublet lines of energy separation $\Delta E = 0.2$ eV at normal emission, the absolute difference in $k_\perp$ is ~0.01 Å^{-1}, which for a typical perovskite lattice constant of $a = 4$ Å is only ~0.5% of the Brillouin zone. The in-plane momentum is

$$k_\parallel = \frac{1}{\hbar}\sqrt{2m_e E_k}\sin(\theta). \tag{8}$$

In the case of $k_\parallel$, assuming a typical emission angle of $\theta = 25°$, the absolute difference in $k_\parallel$ is 0.005 Å^{-1}, less than 0.3% of a typical perovskite Brillouin zone.

The difference in sampled **k** for a typical doublet line is therefore negligible relative to the Brillouin zone, justifying our earlier treatment. Similarly, we would anticipate that differences due to photoemission matrix element effects would also be minimal for the small photon energy differences observed here.

5. Conclusion

We have created a simple method for effectively subtracting the doublet signal's contribution to ARPES spectra in a way that is mathematically straightforward and largely insensitive to noise. This method is advantageous in that the process is more or less universal for any inert gas with higher energy doublet lines, bypassing the need for specific VUV filters. Our quantitative benchmarking of comparative multi-source ARPES data from the non-dispersive misfit compound $(LaSe)_{1.14}(NbSe_2)_2$ demonstrates its viability with regards to the determination of dispersion relations and quasiparticle lifetimes, particularly in 2D and weakly-dispersive non-2D systems. As having access to more photon energies is useful in general, labs with ready access to such multi-gas discharge lamps may benefit from this method at no additional expense. Our approach therefore unlocks numerous doublet emission lines for lab-based ARPES studies on quantum materials.
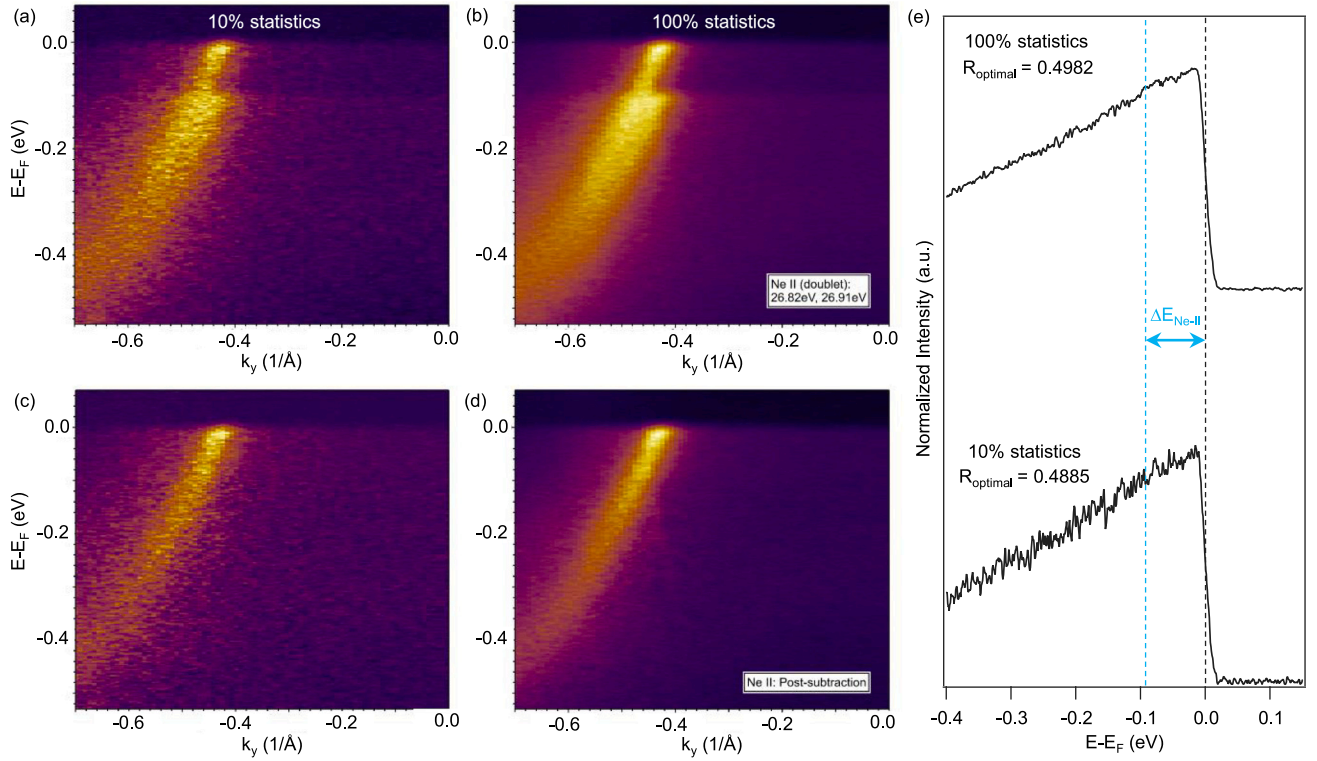
Fig. C.1. (a) Raw spectrum from 10% ARPES scan statistics taken with Ne-II. (b) Raw spectrum from 100% ARPES scan statistics taken with Ne-II. (c) Post-subtracted spectrum of (a). (d) Post-subtracted spectrum of (b). (e) EDCs for the 10% and 100% spectra integrated over a range of k = −0.6 Å^{-1} to k = 0 Å^{-1}.

Declaration of competing interest

The authors declare that they have no known competing financial interests or personal relationships that could have appeared to influence the work reported in this paper.

Data availability

Data will be made available on request.

Appendix A. Measurement of source emission lines

The plasma discharge spectra shown in Fig. 1 were generated via angle-integrated photoemission measurements on a reference polycrystalline gold film, using the identical experimental setup and measurement conditions as for the ARPES data presented throughout the main text. The gold reference sample was generated by e-beam deposition and cleaned via vaccum annealing before being transferred to the ARPES cryostat. For photoemission measurements, the cleaned Au film was held at a temperature of 6 K under good UHV conditions (<7.5 × 10^{-11} Torr), with the electron analyzer set to a nominal energy resolution between 6–10 meV for He-I, Ne-I, Kr, depending on the specific scan. Ne-II data were taken at a nominal energy resolution of 20 meV owing to the reduced signal intensity. In each case, raw integrated EDCs for each noble gas line were obtained, corresponding to the red curves on Fig. A.1. Ar-I, Ne-I, and Ne-II are colored in purple, green, and blue respectively. These curves were then offset by the work function

Table 1
Table of the emission lines shown in Fig. 1, as measured via photoemission from a polycrystalline gold reference sample. Normalized intensities are shown as a percentage of the He-Iα count rate near E_F, and the energies are given as the measured E_F in kinetic energy plus the analyzer work function.

Line	Normalized intensity	Energy (eV)	R (I_β/I_α)
He-I	100%	21.22	–
He-II	0.51%	40.83	–
Kr-I	9.0%	10.02	–
Ar-Iβ	0.47%	11.62	0.28
Ar-Iα	1.7%	11.83	
Ne-Iβ	6.8%	16.67	0.22
Ne-Iα	31%	16.85	
Ne-IIβ	0.30%	26.82	0.40
Ne-IIα	0.76%	26.91	

of our analyzer, 4.32 eV, to give photon energies $h\nu = E_k + \Phi$. Taking the negative of the derivative for the integrated EDCs then produces the relative intensity and shape of the various strong emission lines after convolution with the detector energy resolution, as presented in Fig. 1.

We also tabulate the lines shown in Fig. 1(a) for our system in Table 1 which should be a useful guide for future reference and for anyone who wishes to get an estimate of the various photon energies and relative intensities.

Appendix B. Intensity ratio optimization

Unlike ΔE, R can also vary between experiments using the same system on the same strong emission line due to differences in lamp pressure and monochromator settings. The biggest challenge is that there is no residual to minimize when varying R. Fortunately, even a slightly incorrect R of ±10% of the optimal R value yields a visible

discontinuity in the integrated EDC at ΔE below the Fermi level. To illustrate this, we examined the integrated EDCs extracted from the ARPES spectra of $(LaSe)_{1.14}(NbSe_2)_2$ misfit measured by Ne-I. In Fig. B.1(a), we show the optimal solution from our algorithm in green, which corresponds to the solution using the optimal R value. The orange, pink, blue, and purple curves are the solutions at non-optimal R, which create visible discontinuities in the EDC at $\Delta E = 176$ meV below the Fermi level. Using this fact, we can fit a smooth cubic polynomial in a sub-window straddling the discontinuity, as shown in Fig. B.1(b), which then produces a residual against which the output of our subtraction algorithm can be minimized by varying R. This process of R optimization is shown in Fig. B.1(ai), which plots the χ^2 against the parameter R. Our optimal R value is then the minimum of this optimization curve. We find empirically that choosing the width of this straddling sub-window centered around ΔE to be $\frac{\Delta E}{2}$ works well, and should be generally applicable for avoiding nearby bands which may complicate the process. An alternative method can be implemented utilizing smoothing followed by 2nd derivative analysis in this sub-window. We have chosen a cubic polynomial fit to avoid compounding noise when taking derivatives.

Appendix C. Sensitivity to noise

Here we show that our algorithm performs well even on low ARPES statistics. Using the same data from the $(LaSe)_{1.14}(NbSe_2)_2$, but using 10% and 100% ARPES statistics, allows us to probe our algorithm's sensitivity to noise. In Fig. C.1(c) and (d), we show that the output spectra for 10% and 100% statistics are qualitatively identical. Further examination of the integrated EDCs [Fig. C.1(e)] also show the same quasiparticle peak and line shape. There is no kink in either the low or high statistics EDC at $\Delta E = 90$ meV below the Fermi level corresponding to the doublet energy separation of Ne-II. Additionally, the two optimal R values determined using the method in Appendix B exhibit a fractional difference of under 3%, which attests to the algorithm's consistency even in the presence of worse signal-to-noise ratios.

Appendix D. Code

An implementation of our algorithm written in Igor Pro 7 is available along with example Bi_2Se_3 data shown in Fig. 1(f) at a public Git repository [16].

References

[1] J.A. Sobota, Y. He, Z.-X. Shen, Angle-resolved photoemission studies of quantum materials, Rev. Modern Phys. 93 (2021) 025006.

[2] A. Damascelli, Z. Hussain, Z.-X. Shen, Angle-resolved photoemission studies of the cuprate superconductors, Rev. Modern Phys. 75 (2003) 473.

[3] M. Imada, A. Fujimori, Y. Tokura, Metal–insulator transitions, Rev. Modern Phys. 70 (1998) 1039.

[4] J.W. Harter, P.D.C. King, E.J. Monkman, D.E. Shai, Y. Nie, M. Uchida, B. Burganov, S. Chatterjee, K.M. Shen, A tunable low-energy photon source for high-resolution angle-resolved photoemission spectroscopy, Rev. Sci. Instrum. 83 (2012) 113103.

[5] S. Souma, T. Sato, T. Takahashi, P. Baltzer, High-intensity xenon plasma discharge lamp for bulk-sensitive high-resolution photoemission spectroscopy, Rev. Sci. Instrum. 78 (2007) 123104.

[6] S. Suga, A. Sekiyama, G. Funabashi, J. Yamaguchi, M. Kimura, M. Tsujibayashi, T. Uyama, H. Sugiyama, Y. Tomida, G. Kuwahara, S. Kitayama, K. Fukushima, K. Kimura, T. Yokoi, K. Murakami, H. Fujiwara, Y. Saitoh, L. Plucinski, C.M. Schneider, High resolution, low hv photoelectron spectroscopy with the use of a microwave excited rare gas lamp and ionic crystal filters, Rev. Sci. Instrum. 81 (2010) 105111.

[7] M. Budke, M. Donath, Ar gas discharge lamp with heated LiF window: A monochromatized light source for photoemission, Appl. Phys. Lett. 92 (2008) 231918.

[8] J. Reader, C.H. Corliss, W. Wiese, G. Martin, Wavelengths and Transition Probabilities for Atoms and Atomic Ions, National Standard Reference Data System, 1980.

[9] H. Zhang, C.-X. Liu, X.-L. Qi, X. Dai, Z. Fang, S.-C. Zhang, Topological insulators in Bi2Se3, Bi2Te3 and Sb2Te3 with a single Dirac cone on the surface, Nat. Phys. 5 (2009) 438.

[10] T.J. Reber, N.C. Plumb, J.A. Waugh, D.S. Dessau, Effects, determination, and correction of count rate nonlinearity in multi-channel analog electron detectors, Rev. Sci. Instrum. 85 (2014) 043907.

[11] P. Samuely, P. Szabó, J. Kačmarčík, A. Meerschaut, L. Cario, A.G.M. Jansen, T. Cren, M. Kuzmiak, O. Šofranko, T. Samuely, Extreme in-plane upper critical magnetic fields of heavily doped quasi-two-dimensional transition metal dichalcogenides, Phys. Rev. B 104 (2021) 224507.

[12] R.T. Leriche, A. Palacio-Morales, M. Campetella, C. Tresca, S. Sasaki, C. Brun, F. Debontridder, P. David, I. Arfaoui, O. Šofranko, T. Samuely, G. Kremer, C. Monney, T. Jaouen, L. Cario, M. Calandra, T. Cren, Misfit layer compounds: A platform for heavily doped 2D transition metal dichalcogenides, Adv. Funct. Mater. 31 (2021) 2007706.

[13] A. Nader, A. Lafond, A. Briggs, A. Meerschaut, R. Roesky, Structural characterization and superconductivity in the misfit layer compound (LaSe)1.14(NbSe2), Synth. Met. 97 (1998) 147.

[14] S. Hüfner, Photoelectron Spectroscopy, third ed., Springer, Berlin, Heidelberg, 2003, pp. 39–50, Chap. 1.

[15] Y. Ishida, S. Shin, Functions to map photoelectron distributions in a variety of setups in angle-resolved photoemission spectroscopy, Rev. Sci. Instrum. 89 (2018) 043903.

[16] Y. Tarn, 2023, https://tinyurl.com/SubtractDoublet.